Bending Analysis of Mindlin-Reissner Plates by the Element Free Galerkin Method with Penalty Technique

Yoo Jin Choi, Seung Jo Kim*

Department of Aerospace Engineering, Seoul National University, Seoul 151-742, Korea

In this work, a new penalty formulation is proposed for the analysis of Mindlin-Reissner plates by using the element-free Galerkin method. A penalized weak form for the Mindlin-Reissner Plates is constructed through the exterior penalty method to enforce the essential boundary conditions of rotations as well as transverse displacements. In the numerical examples, some typical problems of Mindlin-Reissner plates are analyzed, and parametric studies on the order of integration and the size of influence domain are also carried out. The effect of the types of background cells on the accuracy of numerical solutions is observed and a proper type of background cell for obtaining optimal accuracy is suggested. Further, optimal order of integration and basis order of Moving Least Squares approximation are suggested to efficiently handle the irregularly distributed nodes through the triangular type of background cells. From the numerical tests, it is identified that unlike the finite element method, the proposed element-free Galerkin method with penalty technique gives highly accurate solution without shear locking in dealing with Mindlin-Reissner plates.

Key Words : EFGM, Meshfree Method, Penalty, Mindlin-Reissner Plate, Shear Locking

1. Introduction

Although the finite element method has served as an industrial standard for solving various kinds of mechanics problems for several decades, the finite element methods have been plagued by its inherent problems such as shear locking, human-labor intensive meshing, severe mesh distortions, etc. Therefore, considerable research efforts have been expended on a meshfree paradigm to get rid of the inherent problems mentioned abore, and as a result various meshfree methods have been extensively developed. Some of these are diffuse element method (DEM : Natroles et al., 1992), element-free Galerkin method (EFGM : Belytschko et al., 1994 ; Belytschko et al., 1996), reproducing kernel particle method (RKPM : Liu et al., 1995 ; Li and Liu, 1999), finite point method (Onate et al., 1996), partition of unity method (PUM : and Melenk, 1997), hp-clouds method (Duarte and Oden, 1996 ; Garcia et al., 2000), meshless local Petrov-Galerkin method (MLPG : Atruli and Zhu , 1998 ; Atruli et al., 1999 ; Atruli and Zhu , 2000), freemesh method (Yagawa and Furukawa, 2000) and others. Meshfree methods have been successfully applied to various engineer ing problems. Related to Mindlin-Reissner plates, Donning and Liu (1998) adopted cardinal spline functions instead of widely used Moving Least Squares interpolation functions. Garcia et al. (2000) analyzed thick plates by hp-clouds method. Cho and Atluri (2001) proposed MLPG method based on locking-free formulation and dealt with shear flexible beams. However, the problem of Mindlin-Reissner plates has not yet been sufficiently dealt with by the meshfree methods such as element-free Galerkin method which is one of the most widely used meshfree methods although the Kirchhoff thin plate was dealt with by element-free Galerkin method in the previous work (Krysl

* Corresponding Author,
E-mail : sjkim@snu.ac.kr
TEL : +82-2-880-7388; **FAX** : +82-2-880-2662
Department of Aerospace Engineering, Seoul National University, Seoul 151-742, Korea. (Manuscript **Received** April 1, 2002; **Revised** October 28, 2002)

and Belytschko, 1996). For this reason, the Mindlin-Reissner plates are analyzed in the present work by applying the element-free Galerkin method.

In the present work, a penalized weak form of Mindlin-Reissner plates for the element-free Galerkin method is introduced by using the exterior penalty method in order to enforce the essential boundary conditions of rotations and displacements. The penalty technique (Zhu and Atluri, 1998) does not introduce additional unknown variables of Lagrange multipliers or cumbersome partial direct transformations (Chen et al., 1997). The numerical examples show that the essential boundary conditions of rotations as well as displacements are effectively enforced through the proposed penalty formulation without much difficultys. Typical problems of Mindlin-Reissner plates are dealt with in numerical examples, and the numerical solutions are compared with analytical solutions. Parametric studies concerning the order of integration and the size of influence domain are carried out, and the dependence of the solutions accuracy on the types of background cells are observed. Based on the investigations, an appropriate type of background cell for obtaining optimal accuracy is suggested. Moreover, since the construction of background integration cell with no regard to the local support of shape function (the influence domain) may result in considerable integration error, special attention should be given to the construction of the integration cell in dealing with irregularly distributed nodes (Dolbow and Belytschko, 1999 ; Park and Youn, 2001 ; Song et al., 2001). Therefore a triangular type background cell is also considered to effectively handle the irregularly distributed nodes (Choi and Kim, 1999 ; Choi et al., 2000). And optimal order of integration and the basis order of Moving Least Squares approximation, which are appropriate for the triangular type background cells, are suggested. From the numerical tests, it is identified that the proposed element-free Galerkin method with penalty technique gives highly accurate solution without shear locking in dealing with Mindlin-Reissner plates in contract to the finite element method.

2. Element Free Galerkin Method with Penalty (EFGMP)

2.1 Moving least squares (MLS) approximation

Suppose that the values of a continuous function $u : \Omega \rightarrow \mathbf{R}$, $\Omega \in \mathbf{R}^n (n=1, 2 \text{ or } 3)$ are given as $\hat{u}_I = u(\mathbf{x}_I)$ at the scattered points $\mathbf{x}_I \in \Omega$ $(I = 1, \cdots, N)$ and the function u in Ω is to be approximated. To approximate the distribution of the function u in Ω, the global approximation form $u^h(\mathbf{x})$ is defined as follows.

$$u(\mathbf{x}) \cong u^h(\mathbf{x}) = \sum_{i=1}^{m} p_i(\mathbf{x})\, a_i(\mathbf{x}) = \mathbf{p}^T(\mathbf{x})\,\mathbf{a}(\mathbf{x}), \quad \text{for all } \mathbf{x} \in \Omega \tag{1}$$

where $\mathbf{p}(\mathbf{x}) = \{ p_1(\mathbf{x}), p_2(\mathbf{x}), \cdots, p_m(\mathbf{x}) \}^T$ is a polynomial MLS basis. The vector $\mathbf{a}(\mathbf{x}) = \{ a_1(\mathbf{x}), a_2(\mathbf{x}), \cdots, a_m(\mathbf{x}) \}^T$ is a vector of undetermined coefficients, whose values can vary according to the position. The coefficient vector $\mathbf{a}(\bar{\mathbf{x}})$ at each position $\mathbf{x} = \bar{\mathbf{x}}$ will be determined by a local weighted least square approximation $u_{\bar{x}}$ of the function $u(x)$, in a sufficiently small neighborhood of $\mathrm{x} = \bar{\mathbf{x}}$. A local weighted least squares approximation $u_{\bar{x}}$ for each point $\bar{\mathbf{x}} \in \Omega$ is given in the following.

$$u_{\bar{x}}(\mathbf{x}) = \sum_{i=1}^{m} p_i(\mathbf{x})\, a_i(\bar{\mathbf{x}}) = \mathbf{p}^T(\mathbf{x})\,\mathbf{a}(\bar{\mathbf{x}}) \tag{2}$$

The coefficient vector $\mathbf{a}(\bar{\mathbf{x}}) = \{ a_1(\bar{\mathbf{x}}), \cdots, a_m(\bar{\mathbf{x}}) \}^T$ is an $m \times 1$ vector that minimizes the following weighted discrete L_2 error norm so that the local approximation is the best approximation to u in the weighted least square sense.

$$J_{\bar{x}}(\mathbf{a}) = \sum_{I=1}^{N} w_I(\bar{\mathbf{x}}) \left[\hat{u}_I - \sum_{i=1}^{m} p_i(\mathbf{x}_I)\, a_i \right]^2 \quad \text{for } \mathbf{a} = \{ a_1, \cdots, a_m \}^T \tag{3}$$

In other words, the coefficient $\mathbf{a}(\bar{\mathbf{x}})$ are found by solving the following problem :

$$\begin{aligned} &\text{Find } \mathbf{a}(\bar{\mathbf{x}}) \equiv \mathbf{a}^* \in \mathbf{R}^m \\ &\textit{such that } J_{\bar{x}}(\mathbf{a}^*) \leq J_{\bar{x}}(\mathbf{a}) \\ &\textit{for all } \mathbf{a} \in \mathbf{R}^m \end{aligned} \tag{4}$$

It is noted that $J_{\bar{x}}(\mathbf{a})$ is dependent on the position $\bar{\mathbf{x}}$. Finally the coefficient vector $\mathbf{a}^*$ can be obtained by the following normalized equation.

$$\sum_{k=1}^{m}\sum_{I=1}^{N} p_j(\mathbf{x}_I)\, w_I(\bar{\mathbf{x}})\, p_k(\mathbf{x}_I)\, a_k(\bar{\mathbf{x}}) = \sum_{I=1}^{N} p_j(\mathbf{x}_I)\, w_I(\bar{\mathbf{x}})\, \hat{u}_I,\ j=1,\ \cdots,\ m \tag{5}$$

Eq. (5) can be rewritten in a simplified matrix form as

$$\mathbf{A}(\bar{\mathbf{x}})\mathbf{a}(\bar{\mathbf{x}}) = \mathbf{B}(\bar{\mathbf{x}})\hat{\mathbf{u}} \tag{6}$$

where

$$\mathbf{A}(\bar{\mathbf{x}}) = \mathbf{P}^T\mathbf{W}(\bar{\mathbf{x}})\mathbf{P} \tag{7}$$

$$\mathbf{B}(\bar{\mathbf{x}}) = \mathbf{P}^T\mathbf{W}(\bar{\mathbf{x}}) \tag{8}$$

In Eqs. (7) and (8), matrix $\mathbf{P}$ is a $N\times m$ matrix, and $\mathbf{W}(\bar{\mathbf{x}})$ is a $N\times N$ diagonal matrix written as follows.

$$\mathbf{P} = [\mathbf{p}(\mathbf{x}_1),\ \mathbf{p}(\mathbf{x}_2),\ \cdots,\ \mathbf{p}(\mathbf{x}_N)]^T \tag{9}$$

$$\mathbf{W}(\bar{\mathbf{x}}) = \begin{bmatrix} w_1(\bar{\mathbf{x}}) & 0 & \cdots & 0 \\ 0 & w_2(\bar{\mathbf{x}}) & \cdots & \vdots \\ \vdots & \vdots & \ddots & 0 \\ 0 & \cdots & 0 & w_N(\bar{\mathbf{x}}) \end{bmatrix} \tag{10}$$

Solving Eq. (6), one can obtain the coefficient vector $\mathbf{a}(\bar{\mathbf{x}})$ as follows.

$$\mathbf{a}(\bar{\mathbf{x}}) = \mathbf{A}^{-1}(\bar{\mathbf{x}})\mathbf{B}(\bar{\mathbf{x}})\mathbf{u} \tag{11}$$

Using the coefficient vector obtained from the local approximation procedure, the global approximation of u given in Eq. (1) can be rewritten as

$$u(\mathbf{x}) = \sum_{j=1}^{m} p_j(\mathbf{x})\, a_j(\mathbf{x}) = \sum_{I=1}^{N} \Phi_I(\mathbf{x})\, \hat{u}_I \tag{12}$$

where

$$\Phi_I(\mathbf{x}) = \sum_{j=1}^{m} p_j(\mathbf{x}) \left(\sum_{k=1}^{m} A_{jk}^{-1}(\mathbf{x})\, p_k(\mathbf{x}_I) \right) w_I(\mathbf{x}) \tag{13}$$

We call that the functions $\Phi_I(\mathbf{x})$ are the MLS shape functions of the approximation. It is noted that $\hat{u}_I\ (I=1,\ \cdots,\ N)$ are not the nodal values of the approximation function $u^h(\mathbf{x})$ but are the given fictitious values of variable u at nodes I. In Eq. (3), $w_I(\mathbf{x})$ is the weight function associated with the position $\mathbf{x}_I$ of node I, $w_I(\mathbf{x})$ is greater than 0 for all $\mathbf{x}$ in the support domain of $w_I(\mathbf{x})$, and N denotes the number of nodes.

The weight function is constructed so that it is positive and the existence of the unique solution $\mathbf{a}(\mathbf{x})$ is guaranteed. The value of $w_I(\mathbf{x})$ is large for points close to the nodal point $\mathbf{x}_I$, and small or zero for points far from the nodal point $\mathbf{x}_I$. In this study, because only the C^0 continuity is required in analyzing the Mindlin-Reissner Plates, the C^0 Gaussian type exponential weight function is utilized, and k_I is taken as 1.

$$w_I(\mathbf{x}) = \begin{cases} \dfrac{\exp(-(d_I/c_I)^{2k_i}) - \exp(-(r_I/c_I)^{2k_i})}{1-\exp(-(r_I/c_I)^{2k_i})}, & d_I \le r_I \\ 0, & d_I \ge r_I \end{cases} \tag{14}$$

where $d_I = \| \mathbf{x}-\mathbf{x}_I \|$ is the distance between position $\mathbf{x}$ and the position of the nodal point $\mathbf{x}_I$. The r_I is the radius of influence domain, and the control parameter c_I is selected as $r_I/4$. It is noted that the present weight functions are differentiable except on the boundary of their supports.

2.2 A penalized weak formulation

In the Mindlin-Reissner plate theory (Timoshenko and Krieger, 1959), the deformation is completely described in terms of the transverse displacement of a middle surface and rotations of the normal to the undeformed middle surface in x-z and y-z planes. The displacements u, v, and w in x-, y-, z-directions assume the following forms.

$$u = -\theta_x z,\ v = -\theta_y z,\ w = w(x,\ y) = w_0 \tag{15}$$

where w_0 is the transverse displacement of the middle surface, θ_x and θ_y are rotations of the normal to the undeformed middle surface in x-z and y-z planes, respectively. By using Eq. (15), the strain field can be also written in terms of the kinematic variables w, θ_x, and θ_y as follows.

$$\boldsymbol{\varepsilon}_b = \begin{Bmatrix} \varepsilon_{xx} \\ \varepsilon_{yy} \\ \gamma_{xy} \end{Bmatrix} = -z \begin{bmatrix} \dfrac{\partial}{\partial x} & 0 \\ 0 & \dfrac{\partial}{\partial y} \\ \dfrac{\partial}{\partial y} & \dfrac{\partial}{\partial x} \end{bmatrix} \begin{Bmatrix} \theta_x \\ \theta_y \end{Bmatrix},$$

$$\boldsymbol{\varepsilon}_s = \begin{Bmatrix} \gamma_{xz} \\ \gamma_{yz} \end{Bmatrix} = \begin{Bmatrix} -\theta_x + \dfrac{\partial w}{\partial x} \\ -\theta_y + \dfrac{\partial w}{\partial y} \end{Bmatrix} \tag{16}$$

where subscripts b and s denote the bending and shear terms, respectively. Further, one can obtain

the stress-strain relationships for the isotropic materials under the plane stress assumption.

$$\boldsymbol{\sigma}_b=\begin{Bmatrix}\sigma_{xx}\\ \sigma_{yy}\\ \sigma_{xy}\end{Bmatrix}=\frac{E}{1-v^2}\begin{bmatrix}1 & v & 0\\ v & 1 & 0\\ 0 & 0 & \frac{1-v}{2}\end{bmatrix}\begin{Bmatrix}\varepsilon_{xx}\\ \varepsilon_{yy}\\ \gamma_{xy}\end{Bmatrix}\equiv\mathbf{E}_b\boldsymbol{\varepsilon}_b,$$
$$\boldsymbol{\sigma}_s=\begin{Bmatrix}\sigma_{xz}\\ \sigma_{yz}\end{Bmatrix}=\begin{bmatrix}G & 0\\ 0 & G\end{bmatrix}\begin{Bmatrix}\gamma_{xz}\\ \gamma_{yz}\end{Bmatrix}\equiv\mathbf{E}_s\boldsymbol{\varepsilon}_s \tag{17}$$

By using the relations given be Eqs. (16) and (17), the total potential energy of the Mindlin-Reissner Plate is written as follows.

$$\Pi=\frac{1}{2}\int_\Omega\boldsymbol{\varepsilon}_b^T\mathbf{D}\boldsymbol{\varepsilon}_b d\Omega+\frac{1}{2}\int_\Omega\boldsymbol{\varepsilon}_s^T\boldsymbol{\alpha}\boldsymbol{\varepsilon}_s d\Omega-\int_\Omega\mathbf{u}^T\mathbf{q}d\Omega-\int_\Gamma\mathbf{u}^T\bar{\mathbf{t}}d\Gamma \tag{18}$$

where $\mathbf{D}=h^3\mathbf{E}_b/12$, $\boldsymbol{\alpha}=t\mathbf{E}_s$, $\mathbf{u}^T=\{\theta_x,\ \theta_y,\ w\}$, $\mathbf{q}^T=\{0,\ 0,\ q\}$, and $\bar{\mathbf{t}}^T=\{\bar{M}_x,\ \bar{M}_x,\ \bar{Q}\}$. Hene, q denotes the distributed transverse force per unit area, and $\bar{Q}$ denotes the prescribed shear force per unit length along the mechanical boundary. $\bar{M}_x$ and $\bar{M}_y$ are the prescribed bending moments per unit length along the mechanical boundary.

As a forementioned, since the penalty technique does not require an additional unknown and preserves favorable matrix structures, the penalty technique is utilized to enforce essential boundary conditions of rotations as well as displacements in this work. For the purpose, the penalized energy is added to the total potential energy of Mindlin-Reissner plates.

$$\Pi_p=\frac{1}{2}\int_\Omega\boldsymbol{\varepsilon}_b^T\mathbf{D}\boldsymbol{\varepsilon}_b d\Omega+\frac{1}{2}\int_\Omega\boldsymbol{\varepsilon}_s^T\alpha\boldsymbol{\varepsilon}_s d\Omega-\int_\Omega\mathbf{u}^T\mathbf{q}d\Omega-\int_{\Gamma_t}\mathbf{u}^T\bar{\mathbf{t}}d\Gamma+\frac{1}{2\varepsilon_p}\int_{\Gamma_u}(\mathbf{u}-\bar{\mathbf{u}})^T(\mathbf{u}-\bar{\mathbf{u}})d\Gamma \tag{19}$$

where ε_p is the penalty parameter, and $\bar{\mathbf{u}}^T=\{\bar{\theta}_x,\ \bar{\theta}_y,\ \bar{w}\}$ denotes the prescribed values of the kinematic variables on the essential boundary. By applying the stationary condition of the penalized total potential energy, the penalized weak form of Mindlin-Reissner plate assumes the form of

$$\delta\Pi_p=\int_\Omega\delta\boldsymbol{\varepsilon}_b^T\mathbf{D}\boldsymbol{\varepsilon}_b d\Omega+\int_\Omega\delta\boldsymbol{\varepsilon}_s^T\boldsymbol{\alpha}\boldsymbol{\varepsilon}_s d\Omega-\int_\Omega\delta\mathbf{u}^T\mathbf{q}d\Omega-\int_{\Gamma_t}\delta\mathbf{u}^T\bar{\mathbf{t}}d\Gamma+\frac{1}{\varepsilon_p}\int_{\Gamma_u}\delta\mathbf{u}^T(\mathbf{u}-\bar{\mathbf{u}})d\Gamma=0 \tag{20}$$

The unknown vectors $\mathbf{u}$ and its variation $\delta\mathbf{u}$ in the proposed weak form are approximated by the moving least square interpolants $\mathbf{u}^h=\boldsymbol{\Phi}\hat{\mathbf{u}}$ and $\delta\mathbf{u}^h=\boldsymbol{\Phi}\delta\hat{\mathbf{u}}$, respectively. Through the moving least square method, the strain vector $\boldsymbol{\varepsilon}_b$ and $\boldsymbol{\varepsilon}_s$ can be also approximated as $\boldsymbol{\varepsilon}_b^h=\mathbf{B}_b\hat{\mathbf{u}}$ and $\boldsymbol{\varepsilon}_s^h=\mathbf{B}_s\hat{\mathbf{u}}$, respectively. Substituting the interpolants into the penalized weak form, Eq. (20) reduces to

$$\delta\hat{\mathbf{u}}^T(\mathbf{K}+\mathbf{K}_p)\hat{\mathbf{u}}=\delta\hat{\mathbf{u}}^T(\mathbf{f}+\mathbf{f}_p),\ \text{for all}\ \delta\hat{\mathbf{u}} \tag{21}$$

Finally we can obtain the following system of linear algebraic equations, Eq. (22), since Eq. (21) holds for all $\delta\hat{\mathbf{u}}$.

$$(\mathbf{K}+\mathbf{K}_p)\hat{\mathbf{u}}=(\mathbf{f}+\mathbf{f}_p) \tag{22}$$

where $\mathbf{K}$ is the stiffness matrix, $\mathbf{K}_p$ is the matrix related to penalty, $\mathbf{f}$ is the load vector, and $\mathbf{f}_p$ is the vector concerning the penalty. The matrices and vectors assume the forms of

$$\mathbf{K}=\int_\Omega\mathbf{B}_b^T\mathbf{D}\mathbf{B}_b d\Omega+\int_\Omega\mathbf{B}_s^T\boldsymbol{\alpha}\mathbf{B}_s d\Omega \tag{23a}$$
$$\mathbf{K}_p=\frac{1}{\varepsilon_p}\int_{\Gamma_u}\boldsymbol{\Phi}^T\boldsymbol{\Phi}d\Gamma \tag{23b}$$
$$\mathbf{f}=\int_\Omega\boldsymbol{\Phi}^T\mathbf{q}d\Omega+\int_{\Gamma_t}\boldsymbol{\Phi}^T\bar{\mathbf{t}}d\Gamma \tag{23c}$$
$$\mathbf{f}_p=\frac{1}{\varepsilon_p}\int_{\Gamma_u}\boldsymbol{\Phi}^T\bar{\mathbf{u}}d\Gamma \tag{23d}$$

2.3 Background cell for numerical integration

To integrate the weak form, most of the mesh-free methods including the element-free Galerkin method construct the background integration cells which are independent of the nodes. The background integration cells have the following features as discussed in Belytschko et al. (1996): The background cells do not need to be compatible with nodes and may be arranged in a regular pattern. The cells serve not only to provide a data structure for the numerical integration but

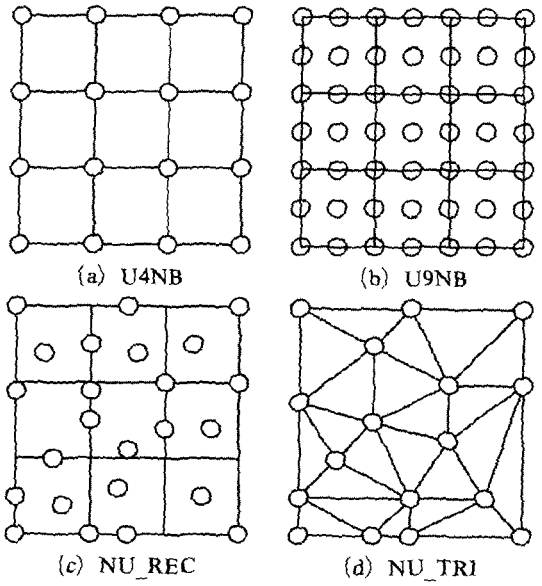

Fig. 1 Types of background cells. (a) 4-node type background cell for uniform node distribution. (b) 9-node type background cell for uniform node distribution. (c) Rectangular type background cell for non-uniform node distribution. (d) Triangular type background cell for non-uniform node distribution

also to facilitate the identification of nodes. The types of background cells that are used in meshfree methods are the cell quadrature type or element quadrature type. In this study, we will consider the four types of background cells as shown in Fig. 1, and investigate the effect of the type of background cell on the solution accuracy.

3. Numerical Experiments

The proposed method is tested by benchmarking examples such as problems of square plates under uniform transverse loads. To compare the solutions obtained by the present element-free Galerkin method with the ones obtained by the finite element methods, the same number of degrees of freedom was adopted in both methods. A Poisson's ratio of 0.3 and Young's modulus of 300 GNm^{-2} were used throughout the tests. And the analytical solution of the classical thin plate theory (Timoshenko and Krieger, 1959) is utilized in assessing the accuracy of each method.

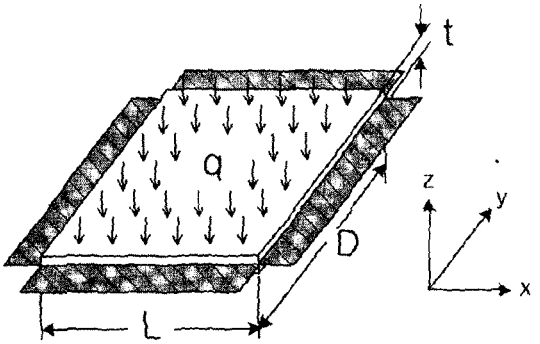

Fig. 2 Clamped square plate subjected to uniform transverse loading

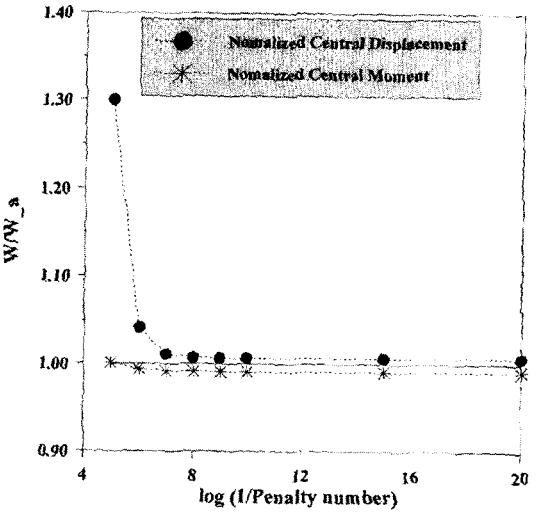

Fig. 3 Convergence for different penalty parameters for clamped square plate

3.1 Test for enforcing the essential boundary condition

Since the MLS shape functions for the nodal points inside the domain may not vanish on the boundary of the domain, it is difficult to handle the essential boundary condition in meshfree methods. In this section, we analyzed a homogeneous clamped square plate under uniform transverse loading, and investigated whether the essential boundary conditions is successfully enforced through the proposed penalty formulation.

A square plate, which is clamped along the four edges subjected to uniform transverse loading as shown in Fig. 2, is analyzed. The thickness t of the plate is 0.01 m, and the edge length L is 1 m.

The model has $17\times17(=289)$ uniform node distribution, and the type of background cells utilized in the analysis is the same type as shown in Fig. 1(b).

The convergence of the displacement and moment at the center point of the plate for different reduces of penalty parameter is presented in Fig. 3. The numerical results show slight deviations from the analytical solutions since the analytical solutions of classical thin plate theory are used for comparism. However, the result clearly shows that both the displacement and moment at the center of the plate converge as the penalty number is decreased. In Fig. 4, the solutions at the essential boundaries for different penalty parameters are presented. The results identify that the proposed method enforces not only the prescribed displacements but also the prescribed rotations successfully.

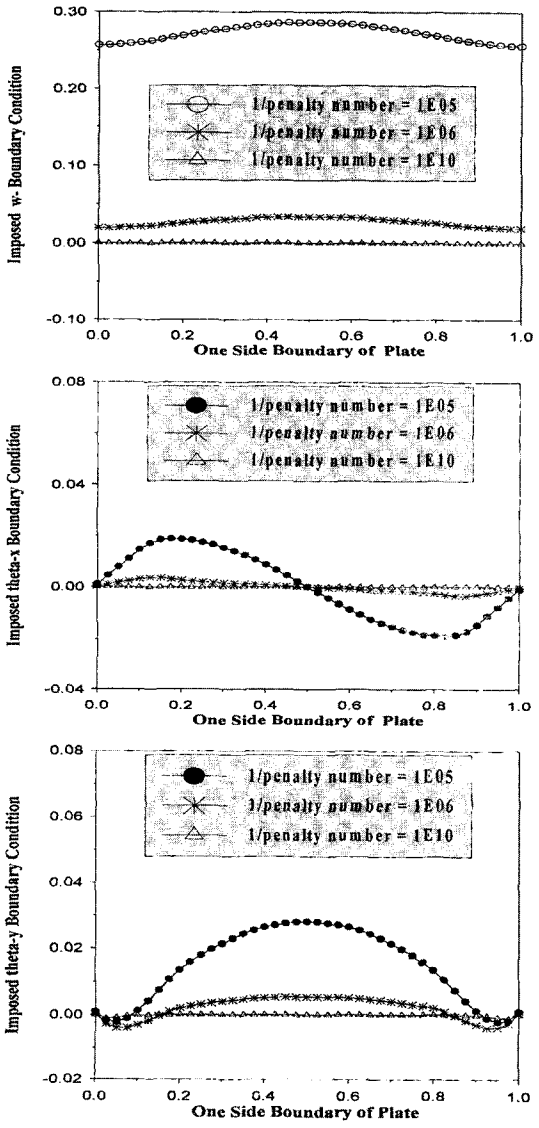

Fig. 4 Enforcement of clamped boundary conditions for different penalty numbers

3.2 Parameteric study

In this section, the parameter studies were carried out with particular focus on the relation between the type of the background cells and the number of integration points per cell (i.e. order of Gaussian quadrature), and also between the total number of nodes and the order of Gaussian quadrature. First, a thin square plate with thickness-to-length ratio of 0.01 is analyzed and the obtained results are presented in Figs. 5 and 6. For meshfree discretization, $17\times17(=289)$ regularly distributed nodes are used, and 4 times the nodal distance is adopted as a radius of support of MLS shape function. In Fig. 5, the effect of the number of integration points per cell (i.e. order of Gaussian quadrature) on the numerical solution is presented for several combinations of the background cells and MLS basis order. It is clearly

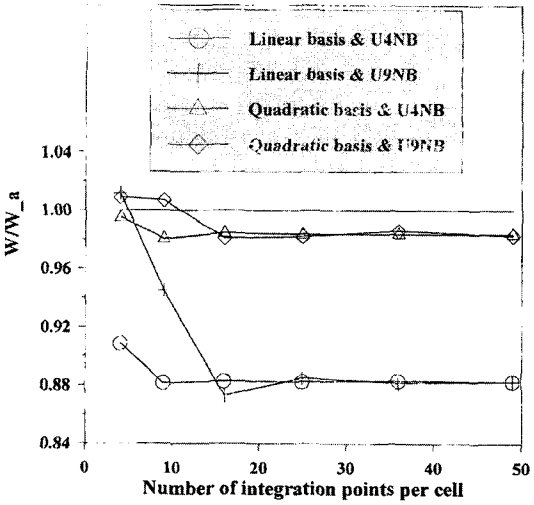

Fig. 5 Effect of MLS basis and background cell on the numerical solutions according to integration orders

shown form the results that the quadratic MLS basis gives much more accurate solution than the one obtained by the linear MLS basis regardless of the order of the Gaussian quadrature (the number of integration points per cell). The results also show that the accuracy of all of the combinations tend to deteriorate the order of the Gaussian quadrature is increased. Further, one can observe that the combination of the quadratic MLS basis and the U9NB type background cell with 3×3 Gaussian quadrature rule (9 integration points) gives the best solution among all the combinations considered in the example. In Fig. 6, numerical solutions according to the order of the Gaussian quadrature (number of integration points per cell) are presented for three cases in which the total number of nodes are different from each other. To calculate the results presented in Fig. 6, the quadratic MLS basis and the U9NB type of background cells are adopted. The results show clearly that regardless of the order of the Gaussian quadrature, the solution becomes stable and the accuray is improved as the total number of nodes is increased. From the results, it is found that the quadratic MLS basis and the U9NB type background cell with 3×3 Gaussian quadrature rule (9 integration points) are the optimal combination for analyzing the Mindlin-Reissner plates in case of uniform node distribution.

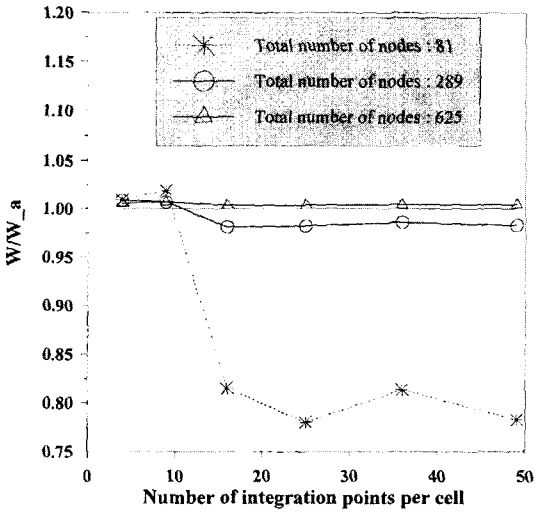

Fig. 6 Effect of total number of nodes on the numerical solutions according to integration orders

Aforementioned in the section of introduction, because the construction of background integration cell with no regard to local support of shape function may result in considerable integration error (Atluri et al., 1999 ; Dolbow and Belytschko, 1999), special attention should be given to constructing the integration cells in dealing with irregularly distributed nodes. Therefore the type of background cell shown in Fig. 1(c) may induce considerable integration error. For this reason, a triangular type background cell is considered instead of a rectangular type in order to effectively handle the irregularly distributed nodes. In a previous work (Choi and Kim, 1999 ; Choi et al., 2000), it was shown that the triangular type background cell gives more reliable solution for the problems with irregularly distributed nodes compared with the one obtained by the rectangular type background cell. In calculating the results presented in Figs. 7(a) and 7(b), the triangular type background cell is adopted to analyze the model with irregularly distributed nodes. In Figs. 7(a) and 7(b), numerical solutions of transverse deflection and moment for different sizes of influence domain are presented for various combinations of order of quadrature and order of the MLS basis, respectively. The results show that both the transverse deflection and momemt are guite insensitive to the size of influence domain (radius of support of the MLS shape function) if we use the 3 points integration rule with the quadratic MLS basis. From the results, it is found that the combination of 3 points integration rule and the quadratic MLS basis guarantees highly accurate and stable moments as well as transverse deflections, and that the combination of 3 points integration rule and the quadratic MLS basis is highly satisfactory for dealing with irregularly distributed nodes. This combination with the triangular type background integration cell is recommended for the analysis of Mindlin-Reissener plates with irregularly distributed nodes.

3.3 Test for shear locking

In the theory of Mindlin-Reissner plates, the

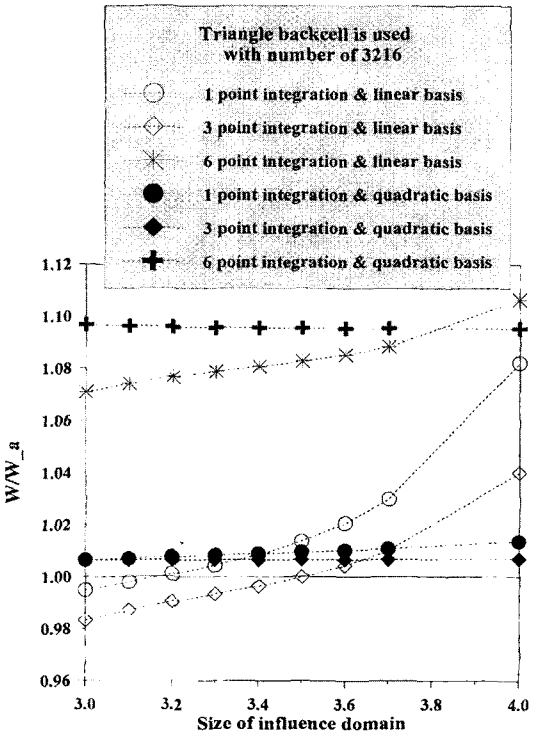

Fig. 7(a) Effect of integration order and the MLS basis on the transverse deflection for different sizes of influence domain: Triangular type background cell is used

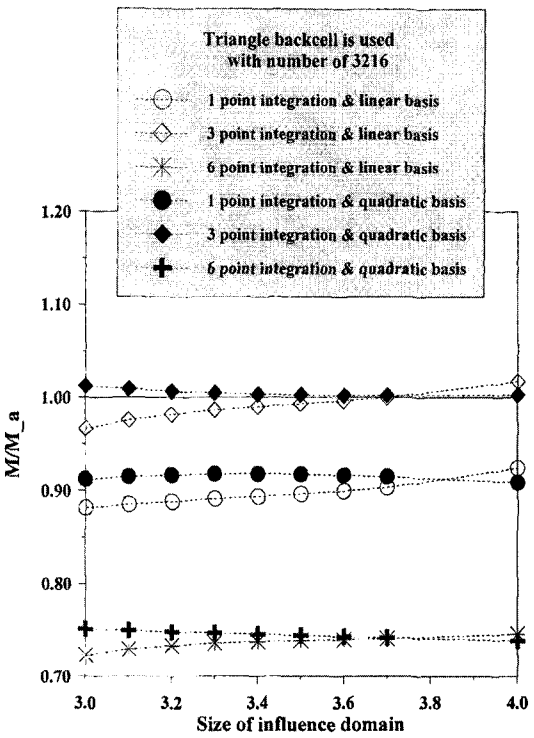

Fig. 7(b) Effect of integration order and MLS basis on the bending moment for differant sizes of influence domain: Triangular type background cell is used

rotations are independent of the transverse displacements, and the transverse shear effects diminish gradually as the plate thickness is decreased. However, if a finite element technique is involved in analyzing thin plates through the theory of Mindlin-Reissner plates, the constraint of almost zero shear strain energy locks the bending motion of the plates and produces wild oscillations in shear stress. This phenomenon is known as "shear locking". Therefore many researchers have concentrated their studies on trying to avoid shear locking through various approaches such as reduced/selective integration, or developing assumed strain elements, among others (H. C. Huang, 1989). Among them, reduced and selective integration schemes are widely used since these integration schemes are simple and efficient. However, they are not universal (H. C. Huang, 1989). Some troubles still remain with reduced/selective integration schemes, and reduced integration induces the spurious kinematic modes which are rather difficult to control.

In this section, two examples involving a 4-edge clamped square plate and a cantilevered plate are analyzed by the proposed EFGMP method in order to investigate whether the shear locking phenomen on vanishes with the proposed EFGMP (Element Free Galerkin Mehtod with Penalty technique).

3.3.1 A cantilevered plate under end load

A cantilevered plate under end load is analyzed by the proposed method, and the results are compared with the results obtained by the finite element method. The geometry of the cantilevered plate, node distribution, and the type of the background cell (U9NB) are presented in Fig. 8. The length-to-width ratio is 8. Fig. 9(a) presents the results obtained by three numerical methods: 4-node finite element with full integration, 4-

node finite element with reduced integration, and EFGMP with linear basis and 3×3 Gaussian quadrature rule (9 integration points per cell). The comparison shows that reasonable results can be obtained without special treatment in the EFGMP case, while the finite element requires special treatment such as reduced integration in order to obtain a reasonable solution in the thin plate region ($L/t>>1$).

In Fig. 9(b), the result obtained by EFGMP is compared with the results obtained by the 9-node finite element. In EFGMP, a quadratic basis and 3×3 Gaussian quadrature rule are adopted. Both of the results presented in Figs. 9(a) and 9(b) clearly identify that EFGMP gives very good solution and does not invokes shear locking in the thin plate region where the length-to-thickness ratio is guite large (even in the region of L/t=10,000).

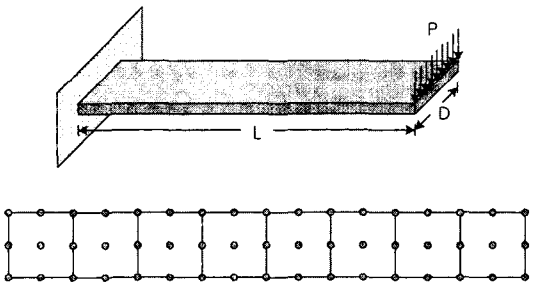

Fig. 8 Cantilevered plates under tip load, nodal distribution and type of background cell (U9NB)

3.3.2 The clamped square plate under uniform lateral load

The clamped square plate subjected to uniform transverse loading is considered in this example. To analyze the problem by the proposed EFGMP, the U9NB type of background cell in Fig. 1(b) is adopted, and in each background cell, 3×3 Gaussian quadrature rule (9 integration points) is utilized to integrate the weak form. To model the clamped plate, uniformly distributed 81 (9×9) nodes are used. In the case of the finite element, the plate is modeled by 8×8 meshes.

In Figs. 10(a), 10(b), and 10(c), the linear basis, quadratic basis, and cubic basis are adopted for MLS approximation, respectively. To compare the results obtained by the proposed EFGMP method with the solutions obtained by the finite elements, 4-node, 9-node, and 16-node elements are utilized in Figs. 10(a), 10(b), and 10(c), respectively. The total numbers of finite element nodes in Fig. 10(a), 10(b), and 10(c) are 81 (=9×9), 289(=17×17) and 625(=25×25), re-

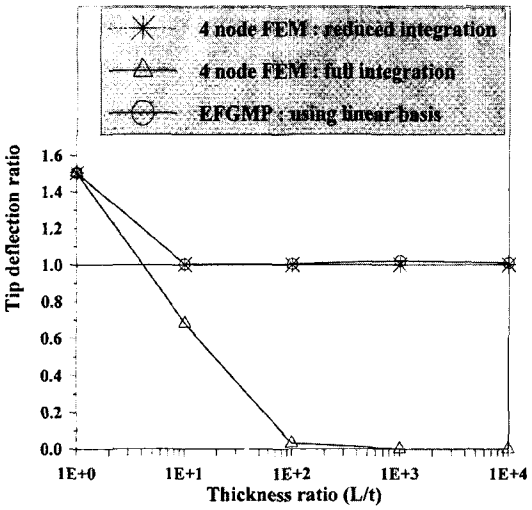

Fig. 9(a) EFGMP with linear MLS basis vs. 4-node finite element : cantilevered plate under tip load

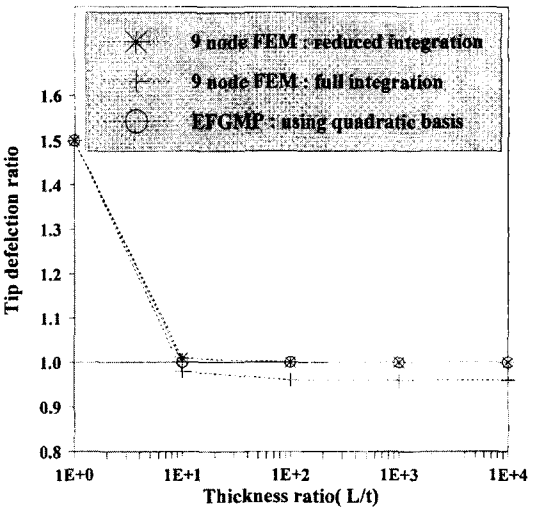

Fig. 9(b) EFGMP with quadratic MLS basis vs. 9-node finite element : cantilevered plate under tip load

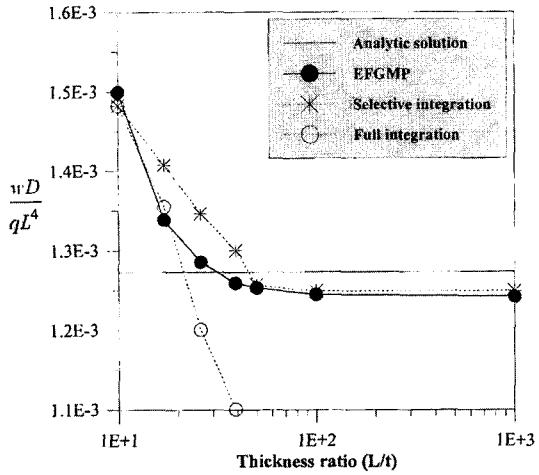

Fig. 10(a) EFGMP with linear basis vs. 4-node finite element: clamped square plate under uniformly distributed transverse load. (D=L)

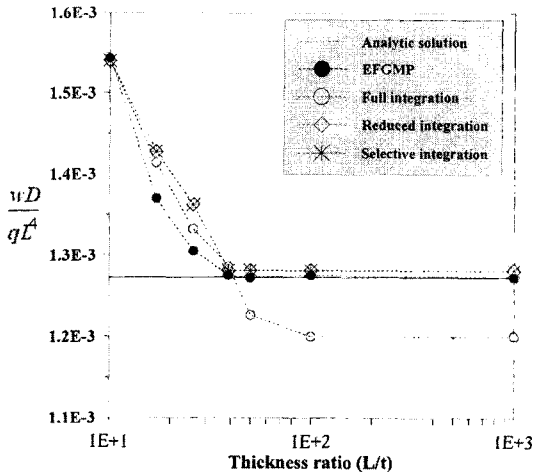

Fig. 10(b) EFGMP with quadratic basis vs. 9-node finite element: clamped square plate under uniformly distributed transverse load. (D=L)

spectively.

In Fig. 10(a), one can observe that the proposed EFGMP method with the linear basis does not invoke a typical shear locking, although the typical shear locking occurs in low order finite elements with full integration. In the higher order case, we can see in Figs. 10(b) and 10(c) that a non-typical locking is not induced in the EFGMP with the quadratic or cubic basis, while

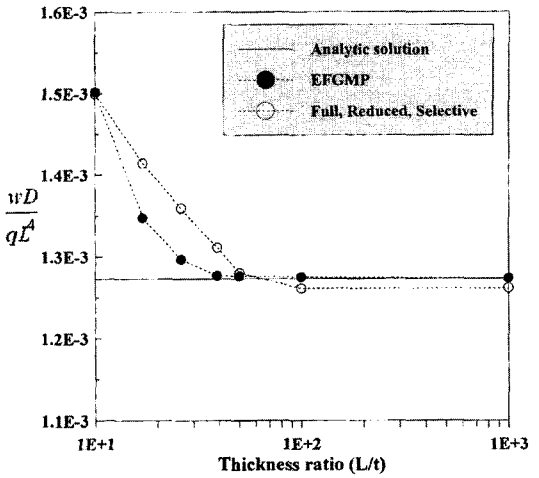

Fig. 10(c) EFGMP with cubic basis vs.16-node finite element : clamped square plate under uniformly distributed transverse load. (D=L)

the higher order element with full integration induces a non-typical locking.

From the results presented in Figs. 10(a) ~ (c), we can confirm that the proposed EFGMP shows much better performance in avoiding shear locking and maintaining the solution accuracy in the thin plate region compared with the finite element methods.

3.4 *Convergence test*

In this section convergence studies are carried out for simply supported and clamped thin plates subjected to uniform transverse loads, and the results are compared with those obtained by the finite element methods that use the same number of nodes.

3.4.1 A simply supported square plate under uniform load

A simply supported square plate under uniformly distributed transverse load was analyzed by the proposed EFGMP. The U9BC type background cell in Fig. 1(b) is adopted, and 3×3 quadrature rule (9 points integration) is utilized. The length-to-thickness ratio L/t of the plate is 100. Using the same number of nodes, the square plate was also analyzed by the QUAD9 element and QUAD9* element (QUAD9 and QUAD9*

Table 1 Convergence of EFGMP : simply-supported square plate under uniformly distributed transverse load

Total number of nodes (U9NB type of background cell)	Deflection at center (W/W_analytic)			Bending Moment at center (M/M_analytic)		
	EFGMP	QUAD9*	QUAD9	EFGMP	QUAD9*	QUAD9
25 (5×5)	1.0145	1.0381	1.0392	1.0450	1.2386	1.2387
81 (9×9)	1.0059	1.0088	1.0089	1.0209	1.0300	1.0300
169 (13×13)	1.0056	1.0076	1.0076	1.0073	1.0109	1.0109
289 (17×17)	1.0053	1.0074	1.0074	1.0028	1.0055	1.0108

Table 2 Convergence of EFGMP : clamped square plate under uniformly distributed transverse load

Total number of nodes (U9NB type of background cell)	Deflection at center (W/W_analytic)			Bending Moment at center (M/M_analytic)		
	EFGMP	QUAD9*	QUAD9	EFGMP	QUAD9*	QUAD9
25 (5×5)	1.0638	2.0791	2.0783	1.0418	1.2246	1.2247
81 (9×9)	1.0418	1.0974	1.0967	1.0378	1.0147	1.0148
169 (13×13)	1.0130	1.0299	1.0293	1.0032	1.0077	1.0077
289 (17×17)	1.0068	1.0114	1.0110	1.0010	1.0066	1.0067

are the 9-node element with reduced integration and the assumed strain element, respectively.), and the results were compared with the solutions obtained by the proposed EFGMP (element-free Galerkin method with penalty technique). Both of the results are presented in Table 1. From the results in Table 1, one can observe that both the deflection and the bending moment at the center of the plate obtained by EFGMP are closer to the analytic solutions of the thin plate theory (Timoshenko and Krieger, 1959) than those obtained by the finite element methods.

3.4.2 A clamped square plate under uniform loads

The uniformly loaded clamped square plate with L/t=100 was analyzed by using the proposed EFGMP. To evaluate the weak form, the U9BC type background cell and 3×3 quadrature rule (9 points integration) are adopted. The results are compared with the solutions obtained by the finite element model with the same number of nodes. The results are presented in Table 2. Similar to the case of a simply-supported plate, the proposed EFGMP shows much improved performance compared with the finite element method.

4. Conclusions

In this paper, a new penalty formulation for the analysis of Mindlin-Reissner plates by the element-free Galerkin method was presented. The penalty formulation enforces the essential boundary conditions on rotations and displacements, where additional unknown variables of the Lagrange multipliers or tedious partial direct transformations can be avoided.

Numerical tests prove that through the proposed penalty formulation the essential boundary conditions on rotations and transverse displacements are efficiently enforced without the loss of desirable matrix properties such as the positive definiteness and banded structure. Some typical problems of Mindlin-Reissner plates are analyzed, and parametric studies an the order of integration and size of the influence domain are performed. Also, the numerical solutions according to the MLS basis order and the types of the background integration cells are investigated.

Based on the numerical results observations, the quadratic MLS basis and 3×3 quadrature rule (9 points integration) with the U9NB type background cell in Fig. 1(b) privide adeguate numerical solutions in the case of uniformly distributed nodes. Further, to handle the irregularly distributed nodes, the triangular type background cell in Fig. 1(d) is introduced, and it is found that accurate and stable solutions are guaranteed by the quadratic MLS basis and three points integration.

The numerical tests concerning the shear locking testify that the element-free Galerkin method with penalty technique gives highly accurate solution and avoids shear locking when applied to Mindlin-Reissner plates unlike the finite element methods. The present element-free Galerkin method with penalty technique has significant advantages over the finite elements in the analysis of Mindlin-Reissner plates.

Acknowledgment

Authors would like to acknowledge the financial support from the Korean Ministry of Science and Technology through the National Research Laboratory Programs under contract number 00-N-NL-01-C-026.

References

Atluri, S. N. and Zhu, T., 1998, "A New Meshless Local Petrov-Galerkin (MLPG) Approach in Computational Mechanics," *Computational Mechanics*, Vol. 22, pp. 117~127.

Atluri, S. N. and Zhu, T., 2000, "New Concepts in Meshless Methods," *International Journal for Numerical Methods in Engineering*, Vol. 47, pp. 537~556.

Atluri, S. N., Cho, J. Y. and Kim, H. G., 1999, "Analysis of Thin Beams, Using the Meshless Local Petrov-Galerkin Method with Generalized Moving Least Squares Interpolations," *Computational Mechanics*, Vol. 24, pp. 334~347.

Babuška, I. and Melenk, J., 1997, "The Partition of Unity Method," *International Journal for Numerical Methods in Engineering*, Vol. 40, pp. 727~758.

Belytschko, T., Lu, Y. Y. and Gu, L., 1994, "Element-Free Galerkin Methods," *International Journal for Numerical Methods in Engineering*, Vol. 37, pp. 229~256.

Belytschko, T., Krongauz, Y., Organ, D., Fleming, M. and Krysl, P., 1996, "Meshless Methods: An Overview and Recent Development," *Computational Methods in Applied Mechanics and Engineering*, Vol. 139, pp. 3~47.

Chen, J. S., Pan, C. and Wu, C. T., 1997, "Large Deformation Analysis of Rubber Based on a Reproducing Kernel Particle Method," *Computational Mechanics*, Vol. 19, pp. 211~227.

Cho, J. Y., Atluri, S. N., 2001, "Analysis of Shear Flexible Beams, Using the Meshless Local Petrov-Galerkin Method Based on a Locking-Free Formulation," *Engineering Computations*, Vol. 18, pp. 215~240.

Choi, Y. J. and Kim, S. J., 1999, "Node Generation Scheme for The Meshfree Method by Voronoi Diagram and Weighted Bubble Packing," *Proceedings of 5th U.S. National Congress on Computational Mechanics*, p. 315.

Choi, Y. J., Chung, S. W. and Kim, S. J., 2000, "Stuny on the Element Free Galerkin Method Using Bubble Packing Technique," *The Transactions of KSME*, Vol. 24, No. 10, pp. 2469~2476.

Dolbow, J. and Belytschko. T., 1999, "Numerical Integration of the Galerkin Weak Form in Meshfree Methods," *Computational Mechanics*, Vol. 23, pp. 219~230.

Donning, B. and Liu, W. K., 1998, "Meshless Methods for Shear Deformable Beams and Plates," *Computer Methods in Applied Mechanics and Engineering*, Vol. 152, pp. 47~72.

Duarte, C. A. and Oden, J. T., 1996, "An h-p Adaptive Method Using Clouds," *Computer Methods in Applied Mechanics and Engineering*, Vol. 139, pp. 237~262.

Garcia, O., Fancello, E. A., Barcellos, C. S. and Duarte, C. A., 2000, "Hp-Clouds in Mindlin's Thick Plate Model," *International Journal for Numerical Methods in Engineering*, Vol. 47, pp. 1381~1400.

Huang, H. C., 1989, Static and Dynamic Analyses of Paltes and Shells: Theory, Software

and Application, Springer-Verlag, Great Britain, pp. 25~71.

Krysl, P. and Belytschko, T., 1996, "Analysis of thin Plates by the Element Free Galerkin Method," *Computational Mechanics*, Vol. 17, pp. 26~35.

Li, S. and Liu, W. K., 1999, "Reproducing Kernel Hierarchical Partition of Unity, Part I: Formulation and Theory," *International Journal for Numerical Methods in Engineering*, Vol. 45, pp. 251~288.

Liu, W. K., Jun, S. and Zhang, Y. F., 1995, "Reproducing Kernel Particle Methods," *International Journal for Numerical Method in Fluids*, Vol. 20, pp. 1081~1106.

Nayroles, B., Touzot, G. and Villon, P., 1992, "Generalizing the Finite Element Method: Diffuse Approximation and Diffuse Element," *Computational Mechanics* ; Vol. 10, pp. 307~318.

Oñate, E., Idelsohn, S., Zienkiewicz, O. C. and Taylor, R. L., 1996, "A Finite Point Method in Computational Mechanics. Applications to Convective Transport and Fluid Flow," *International Journal for Numerical Methods in Engineering*, Vol. 39, pp. 3839~3866.

Park, S. H. and Youn, S. K., 2001, "Least Square Meshfree Method and Integration Error," *The Transactions of KSME*, Vol. 25, No. 10, pp. 1605~1612.

Song, T. H., Seog, B. H. and Lim, J. K., 2001, "Improvement Scheme of Nodal Integration in Meshless Method," *The Transactions of KSME*, Vol. 25, No. 9, pp. 1376~1383.

Timoshenko, S. and Krieger, S. W., 1959, *Theory of Plates and Shells-2nd Edition.*, MaGraw-Hill, New York, pp. 105~123, 180~207.

Yagawa, G. and Furukawa, T., 2000, "Recent Developments of Free Mesh Method," *International Journal for Numerical Methods in Engineering*, Vol. 47, pp. 1419~1443.

Zhu, T. and Atluri, S. N., 1998, "A Modified Collocation Method and a Penalty Formulation for Enforcing the Essential Boundary Conditions in the Element Free Galerkin Method," *Computational Mechanics*, Vol. 21, pp. 211~222.